Low-energy effective theory of Fermi surface coupled with U(1) gauge field in 2+1 dimensions

Sung-Sik Lee
Department of Physics and Astronomy, McMaster University, Hamilton, Ontario, Canada L8S 4M1
(Received 16 June 2009; published 1 October 2009)

We study the low-energy effective theory for a non-Fermi-liquid state in 2+1 dimensions, where a transverse U(1) gauge field is coupled with a patch of Fermi surface with N flavors of fermion in the large N limit. In the low-energy limit, quantum corrections are classified according to the genus of the two-dimensional surface on which Feynman diagrams can be drawn without a crossing in a double line representation and all planar diagrams are important in the leading order. The emerging theory has the similar structure to the four-dimensional SU(N) gauge theory in the large N limit. Because of strong quantum fluctuations caused by the abundant low-energy excitations near the Fermi surface, low-energy fermions remain strongly coupled even in the large N limit. As a result, there are infinitely many quantum corrections that contribute to the leading frequency dependence of the Green's function of fermion on the Fermi surface. On the contrary, the boson self-energy is not modified beyond the one-loop level and the theory is stable in the large N limit. The nonperturbative nature of the theory also shows up in correlation functions of gauge-invariant operators.

DOI: 10.1103/PhysRevB.80.165102 PACS number(s): 71.27.+a, 71.10.Hf, 11.15.Pg

I. INTRODUCTION

Understanding non-Fermi-liquid states is one of the central problems in condense-matter physics. One way of obtaining non-Fermi liquids is to couple a Fermi surface with a massless boson. If a massless boson is associated with criticality achieved by fine tuning of microscopic parameters, a non-Fermi-liquid state arises at a quantum critical point. Such non-Fermi-liquid states have been observed in heavy fermion compounds near magnetic quantum critical points.[1–3] On the other hand, a boson can be dynamically tuned to be massless, and a non-Fermi-liquid state may occur within a finite parameter space. The latter case may arise in the half-filled Landau level of quantum Hall systems[4] and some spin liquid states.[5]

Non-Fermi-liquid states in 2+1 dimensions are of particular interest. Experimentally, high-temperature superconductors which exhibit non-Fermi-liquid behaviors in the strange metallic normal state[5] are quasi-two dimensional. There also exist two-dimensional (2D) frustrated magnets[6,7] whose ground states may be related to a non-Fermi-liquid state of fermionic spinons which carry only spin half but no charge.[8] In the spin liquid state, fermionic spinons form a Fermi surface which is minimally coupled with an emergent U(1) gauge field.[9,10] The transverse component of the gauge field remains gapless at low energies because it is not fully screened by particle-hole excitations. The long-range interaction mediated by the transverse gauge field leads to a non-Fermi-liquid state.[4,11–15] The same low-energy effective theory can arise in various microscopic models, such as frustrated boson systems.[16] Fermi surface of spinless charged fermion coupled with U(1) gauge field has been also proposed for underdoped cuprates.[17] On the theoretical side, two space dimension is special in that it is high enough to have an extended Fermi surface, while it is low enough to support strong quantum fluctuations in the low-energy limit. As a result of strong quantum fluctuations and infinitely many gapless excitations on an extended Fermi surface, it is expected that a nontrivial interacting quantum field theory, which is very different from relativistic quantum field theories, can emerge in the low-energy limit. Even if the non-Fermi-liquid state turns out to be unstable against other more conventional states,[18,19] the physics within a significant temperature range will be inherited from the unstable non-Fermi-liquid state and it is still important to understand the parent non-Fermi-liquid state.

Considerable studies have been devoted to the low-energy effective theory of Fermi surface coupled with U(1) gauge field in 2+1D.[12–16] In this system, there is no controllable parameter other than the number of fermion flavors N. Therefore it is natural to attempt to develop a perturbative expansion in terms of $1/N(N)$ in the large (small) N limit.[12,13,15,16] Based on the computation of some leading-order diagrams, it has been suggested that the $1/N$ expansion is well defined and the low-energy limit is described by a stable interacting theory in the large N limit. The purpose of this paper is to study the low-energy effective theory of the non-Fermi-liquid state more systematically in the large N limit. The key result of the paper is that the theory is not in a perturbative regime even in the large N limit because there are infinitely many leading-order quantum corrections for vertex functions of fermions residing on the Fermi surface. This conclusion has been reached by a systematic classification of quantum corrections in the $1/N$ expansion. Strong quantum fluctuations associated with the infinitely many gapless excitations and the absence of the Lorentz symmetry make the classification very different from relativistic quantum field theories. The theory remains strongly coupled in the low-energy limit and even the leading-order quantum corrections cannot be summed in a closed Dyson equation which can be truncated with a finite number of vertex corrections.

The paper is organized in the following way. In Sec. II, we start by constructing a minimal local action [given in Eq. (5)] that captures the universal low-energy physics of the 2+1-dimensional non-Fermi-liquid state. The minimal action is a renormalizable theory through which one can probe the universal low-energy physics at any (finite) energy scale by sending all UV cutoff and crossover scales to infinity. This

makes the analysis of the low-energy physics more transparent because all nonuniversal elements of the theory have been stripped away from the minimal action. The peculiar property of the present nonrelativistic theory with Fermi surface is that all local time derivative terms are irrelevant in the low-energy limit. Nonetheless one cannot completely drop the time derivative terms from the bare action because if one does so, the theory will not have any dynamics. Therefore one needs to consider a special low-energy limit to retain nontrivial dynamics while keeping only universal properties of the low-energy theory. After we discuss the low-energy limit of the minimal theory, in Sec. III we classify quantum corrections in the large N limit. In Sec. III A, we show that a naive $1/N$ expansion does not work because power of a Feynman graph in N is enhanced in the low-energy limit. This is due to strong quantum fluctuations enhanced by abundant gapless particle-hole excitations near the Fermi surface. More specifically, the leading frequency dependence of the fermion propagator is of the order of $1/N$. Due to the suppressed frequency dependence, magnitudes of Feynman diagrams are enhanced whenever there exists a channel for virtual particle-hole excitations to remain on the Fermi surface. Based on this observation, in Sec. III B, we show that general Feynman diagrams are classified according to the genus of a 2D surface on which Feynman diagrams are drawn without a crossing in a double line representation. Here the double line representation is useful, not because gauge boson or fermions carry a doubled quantum number, but because it allows one to easily count in how many ways particle-hole excitations can remain on the Fermi surface. In particular, when a fermion is on the Fermi surface, the fermion propagator is enhanced to the order of N due to the suppressed frequency dependence. If there are n closed single-line loops in the double line representation, all virtual particle-hole excitations can remain right on the Fermi surface no matter what n components of internal momenta are. The abundant low-lying excitations give rise to an enhancement factor with a positive power of N in proportion to the number of independent channels via particle-hole excitations remain on the Fermi surface. Due to the enhancement factor, there exist infinitely many leading-order quantum corrections for vertex functions of fermions on the Fermi surface. In particular, one has to sum over infinitely many planar diagrams to compute the leading frequency dependence of the fermion propagator. Although fermions on the Fermi surface are strongly coupled, the boson propagator is not modified beyond the one-loop level in the large N limit due to a kinematical constraint.

The genus expansion of Feynman diagrams in the present non-Fermi-liquid state is very similar to that of the four-dimensional SU(N) gauge theory in the large N limit.[20] In both theories, strong quantum fluctuations make all planar diagrams to contribute to the quantum effective action in the leading order of the $1/N$ expansion. However, the physical origins for strong quantum fluctuations are very different between the two theories. In the SU(N) gauge theory, it is due to fluctuations of color degrees of freedom in the internal space while in the present theory, it is due to fluctuations of the extended Fermi surface in the momentum space.

In Sec. IV, we study the dynamical properties of the theory in the large N limit. It is shown that there is no UV divergence in individual planar diagrams. As a result, the theory is stable and there is no quantum correction to the scaling dimension of fermion beyond one-loop order if the summation of individually finite planar diagrams are finite. In Sec. V, we discuss how the nonperturbative nature of the theory manifests itself in correlation functions of a gauge-invariant operator.

II. MINIMAL THEORY AND LOW-ENERGY LIMIT

A. Minimal local action

We consider N flavors of fermion with Fermi surface coupled with a U(1) gauge boson in 2+1D. In the low-energy limit, fermions whose velocities are not parallel or antiparallel to each other are essentially decoupled because (1) fermions are strongly coupled only with the boson whose momentum is perpendicular to the Fermi velocity for a kinematic constraint and (2) the angle that parametrizes Fermi surface acquires a positive anomalous scaling dimension, becoming a decompactified variable which runs from $-\infty$ to ∞ in the low-energy limit.[21] As a result, two fermions which have different Fermi velocities cannot interact with each other through any finite number of scatterings with the boson in the low-energy limit.[22] Therefore, in the low-energy effective theory, it is justified to focus fermionic excitations locally in the momentum space. In general, one has to consider all patches in which Fermi velocities are parallel or antiparallel to each other because all of them are strongly coupled with the boson in the same momentum region.

In this paper, we will focus on low-energy fermions near one patch in the momentum space. As we will see, understanding low-energy dynamics in this simplified case is already nontrivial. At the end, we will comment on the applicability of this restricted theory and an extension to general cases which include other patches with opposite Fermi velocity. We consider the Lagrangian density,

$$\mathcal{L} = \sum_j \psi_j^*(\partial_\tau - iv_x\partial_x - v_y\partial_y^2)\psi_j + \frac{e}{\sqrt{N}}\sum_j a\psi_j^*\psi_j + a[-\partial_\tau^2 - \partial_x^2 - \partial_y^2]a, \quad (1)$$

where ψ_j is the fermion of flavor $j=1,2,\ldots,N$. We have chosen the Fermi velocity to be along the x direction at $\mathbf{k}=0$. v_x is the Fermi velocity and $v_y \sim \frac{1}{m}$ determines the curvature of the Fermi surface. The Fermi surface is on $v_x k_x + v_y k_y^2 = 0$ as is shown in Fig. 1. This is a "chiral Fermi surface" where the x component of Fermi velocity is always positive. a is the transverse component of an emergent U(1) gauge boson in the Coulomb gauge $\nabla\cdot\mathbf{a}=0$. We ignore the temporal component of the gauge field which is screened to a short-range interaction. The transverse gauge field is massless without a fine tuning due to an emergent U(1) symmetry associated with the dynamical suppression of instantons.[21,23] e is the coupling between fermions and the critical boson.

In the one-loop order, singular self-energies are generated from the diagrams in Figs. 2 and 3, and the quantum effective action becomes

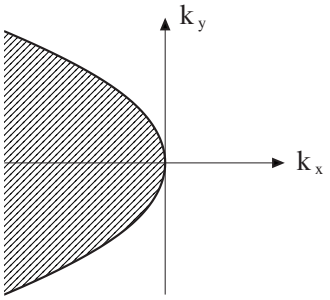

FIG. 1. The parabolic Fermi surface of the model in Eq. (1). The shaded region includes negative-energy states.

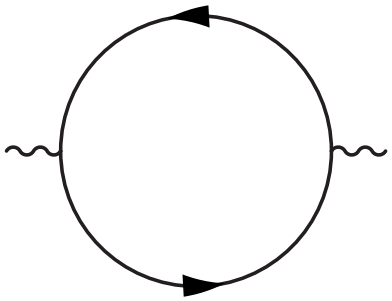

FIG. 2. The one-loop boson self-energy.

$$\Gamma = \sum_j \int dk \left[i\frac{c}{N}\mathrm{sgn}(k_0)|k_0|^{2/3} + ik_0 + v_x k_x + v_y k_y^2 \right] \psi_j^*(k)\psi_j(k) + \int dk \left[\gamma \frac{|k_0|}{|k_y|} + k_0^2 + k_x^2 + k_y^2 \right] a^*(k)a(k) + \frac{e}{\sqrt{N}} \sum_j \int dk dq \;\; a(q)\psi_j^*(k+q)\psi_j(k), \tag{2}$$

where c and γ are constants on the order of 1. To compute the fermion self-energy, the dressed boson propagator has been used because the boson self-energy is on the order of 1. In the low-energy limit, the leading terms of the quantum effective action are invariant under the scale transformation,

$$k_0 = b^{-1}k_0',$$

$$k_x = b^{-2/3}k_x',$$

$$k_y = b^{-1/3}k_y',$$

$$\psi_a(b^{-1}k_0', b^{-2/3}k_x', b^{-1/3}k_y') = b^{4/3}\psi_a'(k_0', k_x', k_y'),$$

$$a(b^{-1}k_0', b^{-2/3}k_x', b^{-1/3}k_y') = b^{4/3}a'(k_0', k_x', k_y'). \tag{3}$$

The singular self-energies render the terms,

$$ik_0\psi_j^*(k)\psi_j(k),$$

$$[k_0^2 + k_x^2]a^*(k)a(k) \tag{4}$$

irrelevant in the low-energy limit. Usually, it is expected that one restores the same low-energy quantum effective action if one drops the irrelevant terms from the beginning. However, this is not true in this case. If one drops the irrelevant terms in the bare action, then the resulting theory becomes completely localized in time and one cannot have a propagating mode. If there is no frequency dependence in the bare action, the frequency-dependent singular self-energies cannot be generated either. Therefore, to restore the full low-energy dynamics, one has to keep the least irrelevant frequency dependent local term. It turns out that the following action given by

$$\mathcal{L} = \sum_j \psi_j^*(\eta\partial_\tau - iv_x\partial_x - v_y\partial_y^2)\psi_j + \frac{e}{\sqrt{N}}\sum_j a\psi_j^*\psi_j + a(-\partial_y^2)a, \tag{5}$$

is the minimal local theory which restores the one-loop quantum effective action [Eq. (2)]. Here η is a parameter which has the dimension $-1/3$ according to the scaling [Eq. (3)].

Since the time derivative term is irrelevant, η will flow to zero in the low-energy limit and the bare value of η does not affect any low-energy physics as far as it is nonzero. The role of the nonzero η is to give a nontrivial frequency-dependent dynamics by maintaining the minimal causal structure of the theory before it dies off in the low-energy limit. For example, in the computation of the one-loop boson self-energy (Fig. 2) in

$$\Pi(q) = e^2 \int d^3k \frac{1}{i\eta(k_0+q_0) + v_x(k_x+q_x) + v_y(k_y+q_y)^2} \frac{1}{i\eta k_0 + v_x k_x + v_y k_y^2} = \gamma\frac{|q_0|}{|q_y|}, \tag{6}$$

the sign of η contains the information on whether the pole is on the upper or lower side in the complex plane for the k_x integration. The final result is independent of η. As far as the "topological" information on the location of poles is kept for the fermions, it generates the correct frequency-dependent self-energy for the boson in Eq. (6). Therefore we can completely drop the time derivative term of the boson in the bare action [Eq. (1)]. The boson self-energy, in turn, generates the frequency-dependent fermion self-energy through Fig. 3.

B. Low-energy limit and large *N* limit

At low energy $k_0 \ll E_\eta$ with $E_\eta = (N\eta)^{-3}$, the dynamically generated fermion self-energy is dominant over the bare term

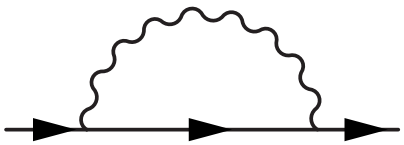

FIG. 3. The one-loop fermion self-energy. Here the boson propagator is a dressed propagator which include the one-loop self-energy correction in Fig. 2.

$i\eta k_0$. Here E_η is a crossover energy scale below which physics is described by the scale-invariant universal theory. To study the low-energy physics, we will fix our energy scale E and send a UV cutoff Λ and the crossover scale E_η to infinity.[24] In taking the low-energy limit, it is convenient to maintain the UV cutoff Λ to be smaller than the crossover scale, that is,

$$E \ll \Lambda \ll E_\eta. \tag{7}$$

First, a Feynman diagram with an external energy E is computed with finite η, Λ and N. To maintain [Eq. (7)], we take the $\eta \to 0$ limit first and then $\Lambda \to \infty$ limit later. Finally, we take the large N limit. This amounts to imposing condition (7) for all N as N is progressively increased in the large N limit. In this way, we can keep the bare time derivative term to be always smaller compared to the singular self-energy at all energy scales. In this limit, not only the IR physics but also the UV physics is controlled by the same universal theory. This is particularly convenient to study universal low-energy dynamics of the theory at the critical dimension which is $d_c=2+1$ in this case. This is because any logarithmic IR divergence is reflected to a UV divergence and one can read the renormalization group flow by keeping track of UV divergences. We will exploit this property to study dynamical properties of the theory in Sec. IV.

The action [Eq. (5)] has four terms which are marginal at the one-loop level. On the other hand, there are five parameters that set the scales of energy momentum and the fields. Out of the five parameters, only four of them can modify the coefficients of the marginal terms because the marginal terms remain invariant under the transformation [Eq. (3)]. Using the remaining four parameters, one can always rescale the coefficients of the marginal terms to arbitrary values. Therefore, there is no dimensionless parameter in this theory except for the fermion flavor N. In the following, we will set $v_x=v_y=e=1$. With this choice, c and γ in Eq. (2) are automatically on the order of 1. The coefficients of the nonlocal terms are not independent tunable parameters because those parameters are completely determined from the local terms.

III. 1/N EXPANSION

A. Failure of a perturbative 1/N expansion

In the naive counting of power in $1/N$, a vertex contributes $N^{-1/2}$ and a fermion loop contributes N^1. In this counting, only the fermion RPA diagram (Fig. 2) is on the order of 1 and all other diagrams are of higher order in $1/N$. In the leading order, the propagators become

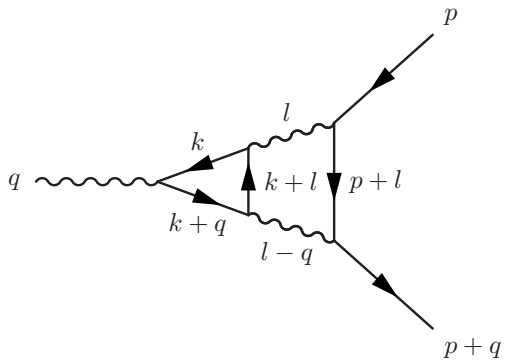

FIG. 4. A two-loop vertex correction.

$$g_0(k) = \frac{1}{i\eta k_0 + k_x + k_y^2},$$

$$D(k) = \frac{1}{\gamma\frac{|k_0|}{|k_y|} + k_y^2}. \tag{8}$$

One can attempt to compute the full quantum effective action by including $1/N$ corrections perturbatively. However, we will see that this naive $1/N$ expansion breaks down in the low-energy limit. To see this, let us consider a two-loop vertex correction shown in Fig. 4,

$$\Gamma(p,p+q) = -N^{-3/2}\int dk dl \;\; g_0(k)g_0(k+q) \times g_0(k+l)g_0(p+l)D(l)D(l-q). \tag{9}$$

Let us focus on the case with $p=0$. Without loss of generality, we can assume $q_0, q_y > 0$. Integrating over k_x, k_y, and l_x, one obtains

$$\Gamma(0,q) = -N^{-3/2}\int dl_0 dl_y dk_0 \frac{F(l_0,l_y,k_0,q_0,q_y)}{l_y\delta_q + i\eta l_y q_0}, \tag{10}$$

where

$$F(l_0,l_y,k_0,q_0,q_y) = 4\pi^3 i[\Theta(l_0+k_0)-\Theta(l_0)] \times [\Theta(k_0+q_0)-\Theta(k_0)] \times [\Theta(q_y-l_y)-\Theta(q_y)]D(l)D(l-q) \tag{11}$$

is a function which is independent of η and N, with $\Theta(x)$ being a step function, and $\delta_q = q_x + q_y^2$ is the "distance" of $\mathbf{q}$ from the Fermi surface. If the final momentum of the fermion is also on the Fermi surface, that is, $\delta_q=0$, the vertex correction becomes

$$\Gamma(0,q) = -\frac{N^{-3/2}}{\eta q_0^{1/3}} f_1(q_y/q_0^{1/3}), \tag{12}$$

where $f_1(t)$ is a nonsingular universal function which is independent of N and η,

$$f_1(t) = 4\pi^3 \int_{-1}^{0} dx \int_{0}^{|x|} dy \int_{1}^{\infty} dz \times \frac{t^2(z-1)}{[\gamma y + (tz)^3][\gamma(1-y) + t^3(z-1)^3]}. \quad (13)$$

In the $\eta \to 0$ limit, this two-loop vertex correction which connects two fermions on the Fermi surface diverges. This divergence is quite generic: a vertex function which connects fermions on the Fermi surface diverges as $1/\eta^n$ for some integer n in general. The physical reason for this divergence is simple. In the $\eta \to 0$ limit, the bare fermion propagator is independent of frequency and the integration over frequencies is ill defined. This divergence is unphysical in the sense that it disappears once the frequency-dependent fermion self-energy correction is included. If one include the one-loop fermion self-energy (Fig. 3), the dressed fermion propagator becomes

$$g(k) = \frac{1}{i\eta k_0 + i\frac{c}{N}\mathrm{sgn}(k_0)|k_0|^{2/3} + k_x + k_y^2} \quad (14)$$

and the $1/\eta$ divergence disappears. Instead, the resulting finite term becomes enhanced by a factor of N^n for some integer $n \geq 0$ because the zero in the denominator (in the $\eta \to 0$ limit) is replaced by a term which is proportional to $1/N$. As a result, the two-loop vertex correction shown in Fig. 4 becomes

$$\Gamma(0,q) = -N^{-1/2} f_2(q_y/q_0^{1/3}), \quad (15)$$

where $f_2(t)$ is a nonsingular universal function which is independent of N and η,

$$f_2(t) = \frac{4\pi^3}{c} \int_{-1}^{0} dx \int_{0}^{|x|} dy \int_{1}^{\infty} dz \frac{1}{|x+1|^{2/3} + y^{2/3} + |x+y|^{2/3} + (z-1)(|x+1|^{2/3} + |x|^{2/3})} \frac{t^2 z(z-1)}{[\gamma y + (tz)^3][\gamma(1-y) + t^3(z-1)^3]}. \quad (16)$$

The additional factor of N is from the enhancement factor that arises due to the $1/\eta$ divergence when the fermions are on the Fermi surface. With the inclusion of the fermion self-energy, the IR divergence in Eq. (12) has been traded with an enhanced power in N in Eq. (15).

Similar enhancement factors arise in other diagrams as well. For example, a three-loop fermion self-energy correction shown in Fig. 5 is on the order of N^{-2} according to the naive counting. However, the self-energy of fermion on the Fermi surface ($\delta_p = 0$) diverges as $1/\eta$ in the $\eta \to 0$ limit if the bare fermion propagator in Eq. (8) is used. If one includes the one-loop self-energy of fermion, it becomes on the order of N^{-1},

$$\Sigma(p) = -i\frac{c_3}{N}\mathrm{sgn}(p_0)|p_0|^{2/3}, \quad (17)$$

when the external fermion is on the Fermi surface. Here c_3 is a universal constant on the order of 1.

This discrepancy between the cases with a finite η and an infinitesimally small η can be understood is the following way. With a finite η, there is a crossover around the scale $q_0 \sim E_\eta$. For $q_0 \gg E_\eta$, the $i\eta k_0$ is dominant in the fermion propagator and a Feynman diagram obeys the naive counting in $1/N$. On the other hand, for $q_0 \ll E_\eta$ quantum fluctuations are controlled by the nonlocal term which is suppressed by $1/N$. The enhanced quantum fluctuations at low energies lead to an enhancement factor by a positive power in N. Since we are concerned about the low-energy physics, we should consider the latter limit. This correct low-energy limit is automatically taken by considering the $\eta \to 0$ limit with a fixed energy scale q_0. This enhancement in the power of N at IR is a manifestation of the fact that quantum fluctuations become stronger at low-energies.

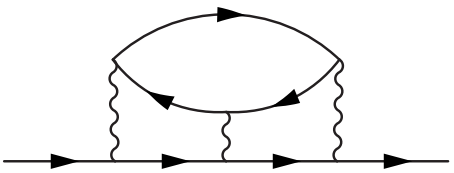

FIG. 5. A three-loop fermion self-energy correction.

B. Genus expansion

In the low-energy limit, what determines the power of a Feynman diagram in $1/N$? To answer this question, one should understand the origin of the enhancement factor discussed in the previous section more systematically. In the present section, we will develop a simple geometrical way of determining power of general Feynman graphs.

First, we illustrate the basic idea using the example (Fig. 4) considered in the previous section. As we have seen in the previous section, the enhancement factor N is a consequence of the $1/\eta$ singularity in the $\eta \to 0$ limit. To understand the origin of the $1/\eta$ singularity, it is useful to examine the way fermions are scattered near the Fermi surface. Suppose both $\mathbf{p}$ and $\mathbf{p}+\mathbf{q}$ are on the Fermi surface in Fig. 4. In the fermion loop with running momentum k, the momentum of the fermion consecutively becomes $k, (k+q), (k+l)$ as a result of scatterings. For a given external momentum q of the boson, one can always choose the spatial momentum $\mathbf{k}$ to make both

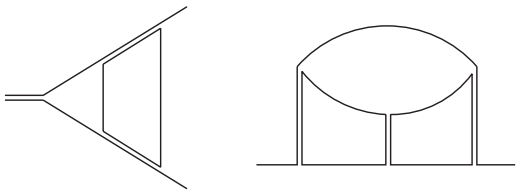

(a) (b)

FIG. 6. The double line representations of Figs. 4(a) and 5(b). Double lines represent propagators of the boson and the single lines are the propagators of the fermion. The number of single-line loops [one in (a) and two in (b)] represents the dimension of the singular manifold (see the text) on which all fermions remain on the Fermi surface in the space of internal momenta.

$\mathbf{k}$ and $\mathbf{k}+\mathbf{q}$ to be on the Fermi surface. There is one unique choice, $\mathbf{k}=\mathbf{p}$. To make the next momentum $\mathbf{k}+\mathbf{l}$ to be on the Fermi surface as well, one needs to tune only l_x and there is one remaining free parameter, l_y. This is because the Fermi surface has dimension one. As a result, all internal fermions can remain right on the Fermi surface during the scattering process no matter what the values of one momentum component (l_y) is if the other three momentum components (k_x, k_y, and l_x) are finely tuned. This implies that all four fermion propagators are singular at $\eta=0$ in an one-dimensional manifold which is embedded in the four-dimensional space $\mathbf{k},\mathbf{l}$. We refer to this manifold as a "singular manifold." The codimension of the singular manifold is $4-1=3$ and there are only three-dimensional integrations which contribute to the phase-space volume and cancel the IR divergence. Since the product of the propagators has a singularity whose strength is 4, the integration over the three parameters cannot completely remove the singularity and the strength of the remaining singularity becomes $4-3=1$. This explains why Fig. 4 has the singularity of $1/\eta$ when the bare fermion propagator is used and why it has the enhancement factor N when the one-loop dressed propagator is used. The enhancement factor N for the fermion self-energy in Fig. 5 can be understood in the similar way.

What determines the dimension of the singular manifold within which fermions always remain on the Fermi surface? It turns out that the dimension of the singular manifold is given by the number of closed loops when one draws boson propagators using double lines and fermion propagators using single lines. This can be shown by following the scheme used to prove the Migdal's theorem in the electron-phonon system.[25,26] First, we restrict momenta of all fermions to be on the Fermi surface. A momentum $\mathbf{k}_\theta$ of fermion on the Fermi surface is represented by an one-dimensional parameter θ. Then, a momentum of the boson $\mathbf{q}$ is decomposed into two momenta on the Fermi surface as $\mathbf{q}=\mathbf{k}_\theta-\mathbf{k}_{\theta'}$, where both $\mathbf{k}_\theta$ and $\mathbf{k}_{\theta'}$ are on the Fermi surface. This decomposition is unique because there is only one way of choosing such $\mathbf{k}_\theta$ and $\mathbf{k}_{\theta'}$ near $\mathbf{k}=0$. As far as momentum conservation is concerned, one can view the boson of momentum $\mathbf{q}$ as a composite particle made of a fermion of momentum $\mathbf{k}_\theta$ and a hole of momentum $\mathbf{k}_{\theta'}$. For example, the two-loop vertex correction in Fig. 4 and the three-loop fermion self-energy correction in Fig. 5 can be drawn as Figs. 6(a) and 6(b), respectively, in this double line representation. In this representation, each single line represents a momentum on the Fermi surface. Momenta in the single lines that are connected to the external lines should be uniquely fixed to make all fermions stay on the Fermi surface. On the other hand, momenta on the single lines that form closed loops by themselves are unfixed. In other words, all fermions can stay on the Fermi surface no matter what the value of the unfixed momentum component that runs through the closed loop is. Since there is one closed loop in Fig. 6(a), the dimension of the singular manifold is 1 and the enhancement factor becomes $N^{4-(4-1)}=N$ for the two-loop vertex correction in Fig. 4. In Fig. 6(b), there are two closed loop and the enhancement factor for Fig. 5 becomes $N^{5-(6-2)}=N$: there are five fermion propagators, six spatial components of internal momenta, and two closed loops.

The enhancement factor is a direct consequence of the presence of infinitely many soft modes associated with deformations of the Fermi surface. The extended Fermi surface makes it possible for virtual particle-hole excitations to maneuver on the Fermi surface without costing much energy. As a result, quantum fluctuations becomes strong when external momenta are arranged in such a way that there are sufficiently many channels for the virtual particle-hole excitations to remain on the Fermi surface. This makes higher order processes to be important even in the large N limit. We note that this effect is absent in relativistic quantum field theories where gapless modes exist only at discrete points in the momentum space.

Now we are ready to write down a general formula which tells order of a general Feynman diagram in $1/N$. (1) First, draw a Feynman diagram using single lines for fermion propagators and using double lines for boson propagators. (2) Second, each vertex contributes $1/\sqrt{N}$. (3) Third, each fermion loop contributes N. (4) Finally, the enhancement factor is given by

$$N^{[I_f-2L+n]}. \tag{18}$$

Here I_f is the number of (internal) fermion propagators, L is the number of loops (the number of internal momenta), and n is the number of closed single-line loops in the double line representation. $[x]=x$ if $x\geq 0$ and $[x]=0$ if $x<0$. This enhancement factor can be understood as was illustrated in the previous examples. When all fermions are on Fermi surface, the product of propagators has the singularity with strength I_f. Upon integrating over the internal momenta, the singularity is lowered due to the contribution from phase-space volume. There are $2L$ components of spatial momenta but n of them are degenerate in that all fermions remain on the Fermi surface no matter what the values of the n momentum components are as far as the remaining $2L-n$ components are zero. Therefore, the integration over the internal momenta can remove the singularity only by the power of $(2L-n)$. The power of the remaining IR divergence is $I_f-(2L-n)$ and this results in the enhancement factor, $N^{(I_f-2L+n)}$. If $(2L-n)>I_f$, the suppression from the phase space of internal momenta is more than enough to suppress the whole singularity and there is no enhancement factor. In this case, the enhancement factor should be 1, not a negative power of N. That is why we

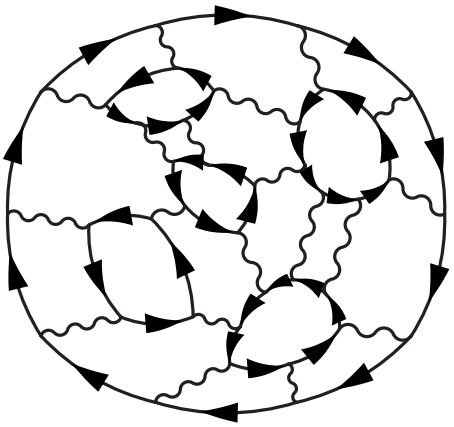

FIG. 7. A typical vacuum planar diagram which is on the order of N^0. In planar diagrams, all fermion propagators which face to each other flow in the opposite direction. In this way, fermions can stay on the Fermi surface before and after scatterings.

use $[I_f-2L+n]$ which is 0 if $I_f<(2L-n)$. By using the relation between L and I_f, $I_f=2L+\frac{E_f+2E_b}{2}-2$, where $E_f(E_b)$ is the number of external fermion (boson) lines, one can write the enhancement factor as

$$N^{[n+(E_f+2E_b)/2-2]}. \tag{19}$$

As a result, the net order of a Feynman diagram is given by N^Q with

$$Q=-\frac{V}{2}+L_f+\left[n+\frac{E_f+2E_b}{2}-2\right], \tag{20}$$

where V is the number of vertices and L_f is the number of fermion loops.

Now let us classify Feynman diagrams based on the expression, Eq. (20), starting from vacuum diagrams. Classification of nonvacuum diagrams with external lines naturally follows from that of vacuum diagrams, as will be shown shortly. The leading-order vacuum diagram is the one fermion loop diagram which is on the order of N. In the next order of N^0, there are infinitely many diagrams. A typical diagram on the order of N^0 is shown in Fig. 7. For the diagram in Fig. 7, we have $V=38$, $n=15$, $E_f=E_g=0$, and $L_f=6$, which gives

$$Q=-19+6+[15-2]=0. \tag{21}$$

Actually, there is a simple geometrical way of interpreting the result. First, we turn fermion propagators into double lines as well by drawing additional single-line loops for each fermion loop as in Fig. 8. In this way, we can include the factor N^{L_f} from fermion loops by counting the additional closed loops of single lines. We will refer to this way of drawing a "full double line representation." If $n\geq 2$, which is always the case for sufficiently large V if there are not too many crossings, we can remove the bracket in Eq. (20) and the power can be rewritten as

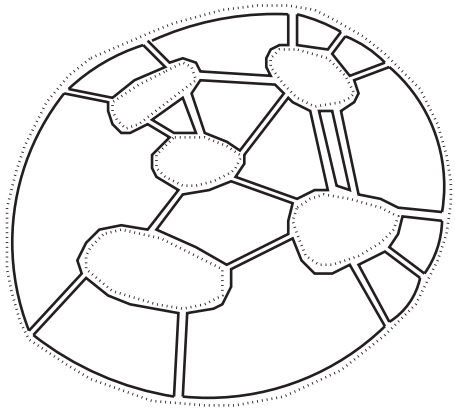

FIG. 8. The full double line representation of the planar diagram shown in Fig. 7. One can draw this diagram on the sphere without any crossing. The solid double lines represent the boson propagator and double lines made of one solid and one dotted lines represent fermion propagators. Loops of dotted lines are added to each fermion loops. In this representation, there is a factor of N for each closed single-line loop whether it is a loop made of a solid or dotted line.

$$Q=V-I+F-2. \tag{22}$$

Here we use the identity $3V=2I$, where I is the number of total internal propagators and $F=n+L_f$ is the total number of single-line loops including the additional single-line loops added to each fermion loop. In this full double line representation, one can think of a closed 2D surface formed by joining the patches of single-line loops. The 2D surface is the surface on which a Feynman diagram can be drawn without any crossing in the full double line representation. The factor $\chi=V-I+F$ is nothing but the Euler number of the 2D closed surface and the power Q becomes

$$Q=-2g, \tag{23}$$

where g is the genus of the 2D surface. The diagrams of the N^0 order are the planar diagrams which can be drawn on a sphere.

For nonplanar diagrams, such as the one shown in Fig. 9,

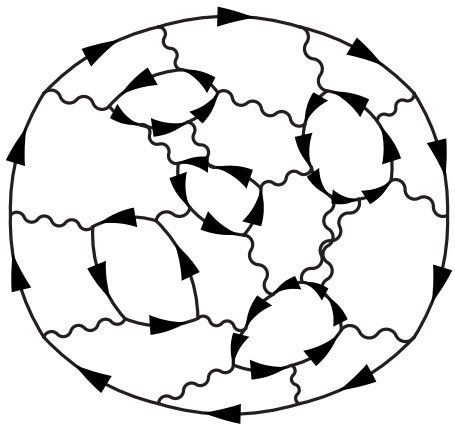

FIG. 9. A nonplanar diagram which is on the order of N^{-2}.

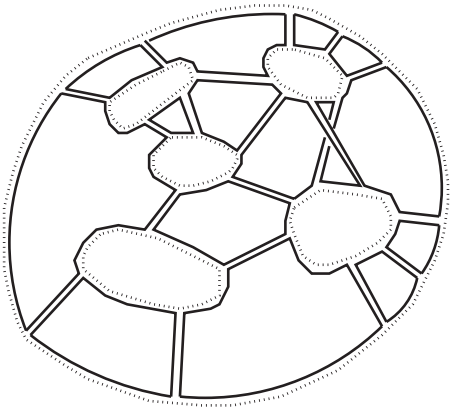

FIG. 10. The full double line representation of Fig. 9. This diagram needs to be drawn on the surface of a torus to avoid a crossing.

one has to introduce closed surfaces with handles to draw them in the full double line representation without a crossing. This is illustrated in Fig. 10. Contributions from nonplanar diagrams are suppressed as the number of genus increases according to Eq. (23).

Power counting of diagrams with external lines can be easily obtained from the counting of vacuum diagrams. To create a boson self-energy diagram, one attaches two vertices to fermion propagators. The leading-order self-energy diagrams can be generated if two vertices are attached to fermion propagators which are parts of one single-line loop. A typical leading-order boson self-energy diagram created from a planar vacuum diagram is shown in Fig. 11. From this procedure, the boson self-energy diagram acquires the additional power of N^{-1} from two added vertices ($\Delta V=2$), N^2 from two external boson lines ($\Delta E_b=2$) and N^{-1} from a lost single-line closed loop ($\Delta n=-1$). As a result, the resulting boson self-energy diagram has the same power as the parent vacuum diagram which is on the order of N^0 for planar diagrams. It is noted that the one-loop boson self-energy diagram (Fig. 2), which can be created by attaching two vertices

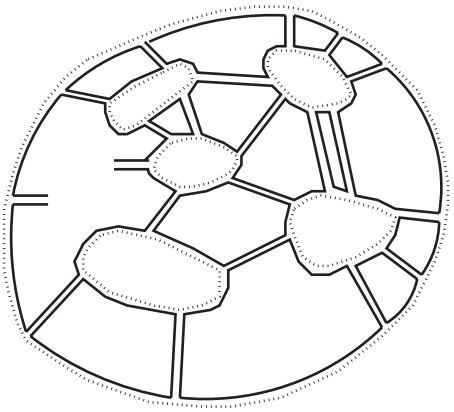

FIG. 11. A boson self-energy diagram drawn in the full double line representation. It has been created by attaching two vertices to the vacuum diagram in Fig. 8. This diagram is nominally on the order of N^0 for any external momentum. But, it turns out that all planar boson self-energy diagrams vanish (see the text).

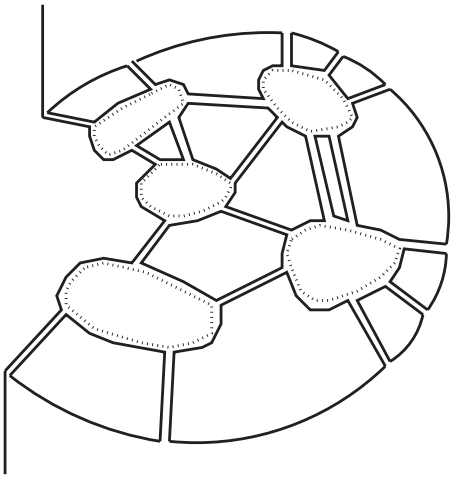

FIG. 12. A fermion self-energy diagram created by cutting fermion propagator open in the vacuum diagram in Fig. 8. This diagram is on the order of N^{-1} when external momentum is on the Fermi surface.

to the vacuum diagram on the order of N, is also order of N^0. Therefore there are infinitely many planar diagrams which contribute to the boson self-energy in the leading order of N^0. If one attaches two vertices to two fermion propagators which belong to different single-line loops or if one starts from a nonplanar vacuum diagram, the resulting boson self-energy is down by an additional factor of $1/N$.

Fermion self-energy diagrams can be created by cutting a fermion propagator as in Fig. 12. This procedure causes an additional power of N^{-1} from one less single-line loop ($\Delta n=-1$), N^1 from two external fermion lines ($\Delta E_f=2$), and N^{-1} from one less fermion loop ($\Delta L_f=-1$). As a result, the fermion self-energy diagram is down by N^{-1} from the vacuum diagram. Therefore the leading-order fermion self-energy corrections are on the order of N^{-1}. There are infinitely many planar diagrams that contribute to the leading frequency dependence of the fermion propagator which is on the order of N^{-1}.

Leading-order three-point vertex functions can be created by cutting a fermion propagator and attaching a vertex to another fermion propagator as in Fig. 13. The resulting diagram is on the order of $N^{-1/2}$: an additional power of $N^{-1/2}$ from $\Delta V=1$, N^{-1} from $\Delta n=-1$, N^2 from $\Delta E_f=2$ and $\Delta E_b=1$, and N^{-1} from $\Delta L_f=-1$. All planar vertex corrections are of the same order as the bare vertex.

For the fermion self-energy and the three-point vertex function, the above counting is valid only when the external fermion momenta are sufficiently close to the Fermi surface. If external momenta are far from the Fermi surface, one cannot make all internal fermions to be on the Fermi surface without an additional tuning of internal momenta. As a result, the enhancement factor becomes smaller than what is predicted for the case when external fermions are on the Fermi surface. To be more precise, Eq. (20) is valid if

$$|\delta_k| \ll \frac{|k_0|^{2/3}}{N}, \tag{24}$$

where k is the momentum of the external fermion. In the opposite limit, $|\delta_k| \gg \frac{|k_0|^{2/3}}{N}$, there are additional factors in $1/N$.

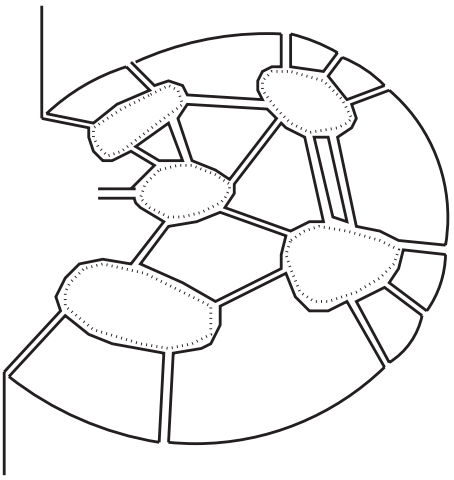

FIG. 13. A vertex correction created by cutting a fermion propagator open and attaching a vertex to the vacuum diagram in Fig. 8. This diagram is on the order of $N^{-1/2}$ when external fermion is on the Fermi surface.

On the other hand, for the boson self-energy, Eq. (20) is always valid, irrespective of the energy and momentum of the external boson. This is because any boson momentum can be decomposed into two momenta on the Fermi surface and one can use the double line representation, which leads to the counting in Eq. (20).

The leading contributions come from the planar diagrams where the genus of the underlying 2D surface is zero. In principle, there can be infinitely many diagrams which are order of $N^0(N^{-1})$ for the boson (fermion) self-energy and $N^{-1/2}$ for the three-point vertex function. In particular, the boson self-energy has infinitely many leading-order terms at any external momentum. This would have made the one-loop boson propagator unreliable even in the large N limit. However, it turns out that all planar diagrams for the boson self-energy correction beyond the one-loop level vanish due to a kinematical reason. To see this, let us consider a three-loop boson self-energy correction shown in Fig. 14,

$$\Pi(q) = -N^{-1}\int dk_1 dk_2 dl \;\; g(k_1)g(k_1+q) \times g(k_1+l)g(k_2)g(k_2+q)g(k_2+l)D(l)D(1-q). \tag{25}$$

This diagram is nominally on the order of N^0 due to an enhancement factor N^1. Integrating over δ_l, one obtains

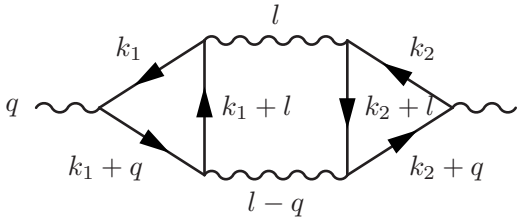

FIG. 14. A planar three-loop boson self-energy.

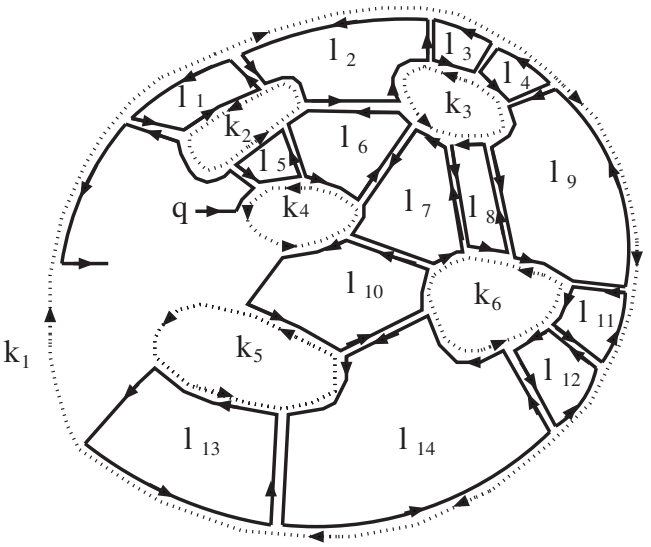

FIG. 15. The assignment of one internal momentum to each closed single-line loop in the boson self-energy diagram in Fig. 11.

$$\Pi(q) \sim \int d\delta_{k_1} d\delta_{k_2} d_{k_{1y}} d_{k_{2y}} dk_{10} dk_{20} dl_0 dl_y D(l)D(l-q) \times \frac{1}{\delta_{k_1} + i\{k_{10}\}} \frac{1}{\delta_{k_1} + \delta_q + 2k_{1y}q_y + i\{k_{10}+q_0\}} \times \frac{1}{\delta_{k_2} + i\{k_{20}\}} \frac{1}{\delta_{k_2} + \delta_q + 2k_{2y}q_y + i\{k_{20}+q_0\}} \times \frac{\Theta(k_{10}+l_0) - \Theta(k_{20}+l_0)}{\delta_{k_1} - \delta_{k_2} + 2(k_{1y}-k_{2y})l_y + i(\{k_{10}+l_0\} - \{k_{20}+l_0\})} \tag{26}$$

with $\delta_k = k_x + k_y^2$ and $\{x\} = \frac{c}{N} x|x|^{-1/3}$. Now we change the integration variables as $k_{1y} = k$ and $k_{2y} = k + k'$. The integration over k has poles at $i\{k_{10}+q_0\}/2q_y$ and $i\{k_{20}+q_0\}/2q_y$, and these poles are on the same side on the complex plane. This can be seen from the fact that

$$|q_0| > \max(|k_{10}|, |k_{20}|, |l_0|). \tag{27}$$

If Eq. (27) is not true, one of $|k_{10}|, |k_{20}|, |l_0|$ should be the largest among all frequencies. If $|k_{10}|$ is the largest, then the integration over δ_{k_1} vanishes because all terms dependent on δ_{k_1} have poles on the same side in the complex plane. This same argument applies to all other frequencies. Therefore Eq. (27) should be satisfied in order for the integrations for δ_{k_1}, δ_{k_2}, and δ_l not to vanish. Then $i\{k_{10}+q_0\}/2q_y$ and $i\{k_{20}+q_0\}/2q_y$ are on the same side in the complex plane and the integration over k vanishes. This proves that Eq. (25) vanishes.

One can easily generalize the previous argument to prove that all planar diagrams for boson self-energy correction vanish. Consider a general boson self-energy diagram shown in Fig. 11. One can arrange internal momenta so that one internal momentum runs within each single-line loop as is shown in Fig. 15. Here k_i's are momenta that run within fermion loops and l_i's are momenta that connects different fermion

loops through boson propagators. If one performs the integrations over δ_{l_i} and changes the integration variables as $\delta_{k_i}=k_{ix}+k_{iy}^2$ for all i, $k_{1y}=k$, $k_{2y}=k+k_2'$, $k_{3y}=k+k_3'$, …, $k_{6y}=k+k_6'$, one can see that k dependencies arise only from $g(k_i+q)$'s. In order for the integrations for δ_{k_i} and δ_{l_i} not to vanish, the external frequency should be the largest of all frequencies in magnitude, that is, $|q_0|>\max(|k_{i0}|,|l_{i0}|)$. As a result, the integration over k has all poles on one side in the complex plane: all q_0+k_{i0} have the same sign as q_0. Therefore all planar diagrams for boson self-energy vanish. The reader may wonder why the one-loop boson self-energy (Fig. 2) does not vanish. This is because the integration over k_y obtained after performing the k_x integration in Eq. (6) has only one pole. This is special for the one-loop diagram and all higher-loop planar boson self-energy graphs vanish.

Although the one-loop result is accurate for the boson self-energy in the large N limit, there are infinitely many nonvanishing planar diagrams for fermion self-energy and vertex correction. This is because in those diagrams there exist "isolated" internal fermion propagators which are not part of any fermion loops (for example, the fermion propagator with momentum $p+l$ in Fig. 4) and the integration over k (the uniform component of k_{iy}) can have poles in both sides in the complex plane due to contributions from the isolated fermion propagators. All planar fermion self-energy diagrams are on the order of N^{-1} and planar vertex corrections are order of $N^{-1/2}$, when external fermions are on the Fermi surface. Since the leading frequency dependence of the fermion propagator is on the order of N^{-1}, one has to sum over all planar diagrams to extract dynamical properties of low-energy fermions. We note that the set of all planar diagrams is much larger than the set of rainbow diagrams that can be summed in a closed Dyson equation.[15] The fact that the low-energy dynamics of fermion is governed by the infinitely many planar diagrams implies that *fermions on the Fermi surface remain strongly coupled even in the large N* limit.

A few comments are in order for Eq. (20). First, the counting of power in $1/N$ is self-consistent in that we obtained Eq. (20) based on the assumption (suggested by the one-loop result) that the leading self-energy corrections of boson and fermion are on the order of N^0 and N^{-1}, respectively. The fact that Eq. (20) predicts the same conclusion implies that the power counting will not change even though one uses the full propagators obtained by summing over all planar diagrams. Second, some nonplanar diagrams may have a higher power in $1/N$ than nominally predicted in Eq. (20) because they can vanish to the leading order due to an even-odd symmetry and there can be $\log N$ correction.[15,27] However, all planar diagrams obey Eq. (20) without $\log N$ correction.

IV. STABILITY AND ANOMALOUS DIMENSION

The coupling e in Eq. (5) receives quantum corrections only from the boson self-energy due to the Ward identity. The absence of nonvanishing planar diagrams for boson self-energy beyond the one-loop level implies that the one-loop beta function is exact in the large N limit.[28] Since the one-loop boson self-energy has no divergence, the beta function is zero and the theory is stable in the large N limit. The fact that the one-loop result is exact is rather remarkable given that the theory remains strongly coupled even in the large N limit. This is consistent with an earlier two-loop calculation.[13] The absence of higher order corrections is reminiscent of supersymmetric theories where certain properties are protected from higher-loop corrections due to the nonrenormalization theorem.[29]

In contrast to the boson, it is difficult to extract detailed dynamical properties of low-energy fermions on the Fermi surface even in the large N limit because there are infinitely many planar diagrams to be considered. However, one can attempt to study the dynamics of fermion on a general ground. Here we will show that there is no UV divergence in all planar diagrams individually, if one uses the one-loop propagators for the computation of higher-order planar diagrams. Of course, the one-loop propagator is not reliable for fermion on the Fermi surface even in the large N limit. The present approach amounts to summing the one-loop self-energy first and then include the rest of the planar diagrams to examine whether there is UV divergence or not.

According to Eq. (3), the scaling dimension of k is given by

$$[k_0]=1, \quad [k_x]=\frac{2}{3}, \quad [k_y]=\frac{1}{3}. \tag{28}$$

Every loop contributes scale 2 and every propagator has scale $-2/3$. Therefore, the superficial degree of divergence of a E-point vertex function is given by

$$D_s=2L-\frac{2}{3}I=2\left(1-\frac{E}{3}\right), \tag{29}$$

where E is the number of external lines, L is the number of loops, and I is the number of internal propagators. Here we have used the relations, $3V=E+2I$ and $L=I-V+1$.

There are three kinds of diagrams which are primitively divergent, that is, diagrams which have generic divergence at UV without divergent subdiagrams. The primitively divergent diagrams are the two-point vertex functions (self-energies) with $D_s=2/3$ and the three-point vertex function ($D_s=0$) which may have power-law and logarithmic divergences, respectively.

Although the superficial degree of divergence suggests that these diagrams are potentially UV divergent, there is actually no divergence for planar diagrams which are dominant in the large N limit. This can be seen from an argument similar to the one that we used to prove that all planar boson self-energy diagrams vanish. For planar diagrams, one can assign an internal momentum k_i for each single-line loop, as we did in Fig. 15. (In contrast to Fig. 15, here we use k_i for all internal momenta to keep the notation for the following discussion simpler.) If external frequency is zero, the integration over δ_{k_i} does not vanish only when

$$|k_{i0}|<\max_{j\in i}(|k_{j0}|), \tag{30}$$

where k_j's are momenta of fermion propagators which are parts of the ith loop. For example, for the integration of δ_{k_2} in Fig. 15 to survive, one should have

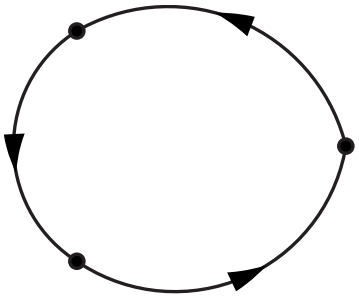

FIG. 16. The one-loop diagram for the three-point density correlation function. The dots represent the density operators.

$$|k_{20}| < \max(|l_{10}|,|l_{20}|,|l_{50}|,|l_{60}|), \tag{31}$$

if $q_0=0$. These set of constraints cannot be simultaneously satisfied for all i's. If one of the internal frequencies, say k_{m0}, is the largest, then the δ_{k_m} integration vanishes because all poles are on the same side in the complex plane. This implies that the volume of frequency integral vanishes when the external frequency vanishes. Since at least one frequency integral has a UV cutoff at an external frequency, the remaining integrations have a reduced degree of divergence which is at most $2/3-1=-1/3$. Therefore there is no UV divergence in all planar diagrams.

If individually finite planar diagrams can be summed to give a finite result, the theory is UV finite in the large N limit. This would imply that the scaling dimension of the fermion field given by Eq. (3) will not be modified by higher-loop diagrams in the large N limit. However, we emphasize that it is not clear whether the summation over planar diagrams is convergent or not. We believe that the true nature of this theory has not been fully understood.

V. CORRELATION FUNCTION OF GAUGE-INVARIANT OPERATORS

Since the fermion operator is not gauge invariant, the fermion Green's function cannot be directly measured. Therefore it is of interest to study how correlation functions of gauge-invariant operators are affected by the fact underlying fermions remain strongly coupled in the low-energy limit. Here we consider correlation functions of the density operator, $\rho(x)=\psi_j^*(x)\psi_j(x)$. The two-point correlation function $\langle\rho(q)\rho(-q)\rangle$ is proportional to the self-energy of the gauge boson. As is shown in Sec. III, all planar boson self-energy diagrams vanish except for the one-loop diagram. Therefore the density-density correlation function shows the usual Fermi-liquidlike behavior in the large N limit.[13] Higher order terms become important only for the n-point density correlation function with $n\geq 3$. Contrary to the two-point correlation function, higher order diagrams for the n-point function with $n\geq 3$ do not automatically vanish. Since there are more than one external frequency, the argument used in Sec. III to show that all planar boson self-energy diagrams with more than one loop vanish does not apply. For example, let us consider the three-point density correlation function given by

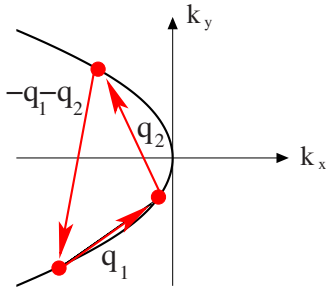

FIG. 17. (Color online) A set of external momenta for which the three-point density correlation function is enhanced. If external momenta are chosen so that all of them connect two points on the Fermi surface, it is possible that all internal fermions stay on the Fermi surface. This gives rise to the divergence $1/\eta$ for the diagram in Fig. 16 if the bare fermion propagator is used. This can be understood following the same argument given in Sec. III. There are three internal propagators which can diverge when $\eta=0$. Since there are only two integrations for the spatial components of internal momenta, a linear divergence survives. Once the fermion self-energy is included, the linear divergence is traded with an enhancement factor N.

$$D_3(q_1,q_2)=\langle\rho(q_1)\rho(q_2)\rho(-q_1-q_2)\rangle. \tag{32}$$

For generic external momenta, the leading contribution is given by the one-loop diagram shown in Fig. 16, which is on the order of N. However, for a set of external momenta which connect points on the Fermi surface, the magnitude of the diagram is enhanced. If the spatial components of the external momenta can be written as

$$\mathbf{q}_1=\mathbf{k}_2-\mathbf{k}_1,$$

$$\mathbf{q}_2=\mathbf{k}_1-\mathbf{k}_3, \tag{33}$$

where $\mathbf{k}_i$'s are momenta residing on the Fermi surface, the diagram is enhanced to the order of N^2. For these special external momenta, there is a channel for all virtual particle-hole excitations to remain on the Fermi surface and there is an enhancement factor N. This is illustrated in Fig. 17. For these external momenta, there are infinitely many planar diagrams which are of the same order. For example, the diagram in Fig. 18 is on the order of N^0 for generic external momenta but it is enhanced to the order of N^2 if external momenta satisfy Eq. (33), as explained in Fig. 19.

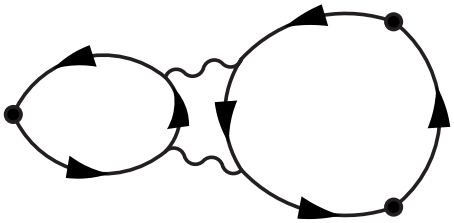

FIG. 18. A three-loop planar diagram which contributes to the leading-order three-point density correlation function when external momenta are chosen so that all of them connect two points on the Fermi surface.

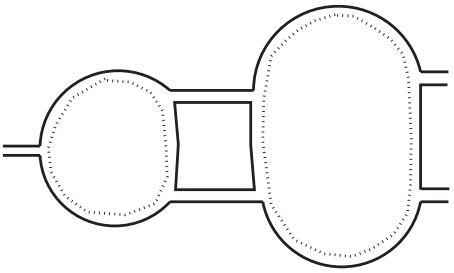

FIG. 19. If the external momenta in Fig. 18 satisfy Eq. (33), every external momentum can be decomposed into two momenta on the Fermi surface. This allows one to draw the diagram in the double line representation as is shown in this figure. There is one loop of solid single line in the double line representation, which implies that there is an one-dimensional singular manifold in the space of internal momenta within which all internal fermions stay on the Fermi surface. As a result, the order of the diagram is given by $Q=-4/2+2+[1+3-2]=2$, where we use $V=4$, $L_f=2$, $n=1$, $E_f=0$, and $E_b=3$ in Eq. (20).

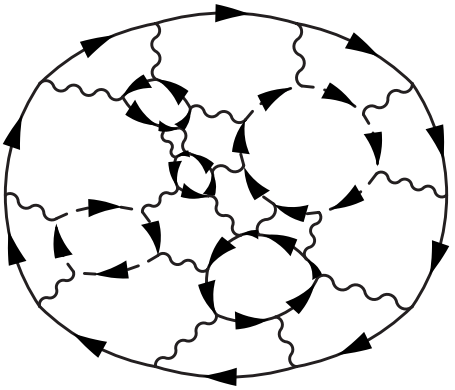

FIG. 20. A planar diagram which include loops of fermions on both sides of the Fermi surface. The solid (dashed) lines represent the propagator of fermions on one (the opposite) side of the Fermi surface. In order for fermions to remain on the Fermi surface, two fermions propagators that face each other should run in the opposite (same) direction if the two fermions are on the same (opposite) side of the Fermi surface.

VI. DISCUSSIONS

A. Comparison with the SU(N) gauge theory

The genus expansion of the present theory is similar to that of the 3+1D SU(N) gauge theory in the large N limit.[20] In the SU(N) gauge theory, all Feynman diagrams can be naturally drawn in the double line representation because the gauge field is in the adjoint representation. Although the physical origin is very different from the present case, nonplanar diagrams with genus g are suppressed by the factor $1/N^{2g}$. One key difference from the present theory is that there is another dimensionless parameter called 't Hooft coupling $\lambda=Ng_{YM}^2$ in the SU(N) gauge theory, where g_{YM} is the gauge coupling. This allows for a double expansion of the theory in $1/N$ and λ. For $\lambda \ll 1$, the theory is in the perturbative regime. In the large N limit with a large but fixed 't Hooft coupling $\lambda \gg 1$, planar diagrams with a large number of loops are dominant and the usual perturbative approach breaks down even in the large N limit. It has been suggested that a more weakly coupled effective description of the theory should be a string theory in an one higher dimensional (4+1D) curved space.[30] The anti-de-Sitter space/conformal field theory (AdS/CFT) correspondence[31–33] is a concrete conjecture of this kind for a supersymmetric SU(N) gauge theory. On the other hand, the present theory with Fermi surface has no 't Hooft coupling that one can tune in addition to N. To put it otherwise, the effective 't Hooft coupling has been set to be on the order of 1. This is because there is no dimensionless parameter in the theory other than N as discussed earlier. With $\lambda \sim 1$, the theory is still strongly interacting but it is most likely not in the regime where one can use a dual gravity description in a weakly curved space time.[34–36] It would be of great interest to find a more weakly coupled description, which is likely to be a gauge-invariant description, for this non-Fermi-liquid state.

B. Extension to multiple patches and applicability of the theory with one patch

In this paper, we have focused on low-energy fermion on one side of Fermi surface (one patch). If Fermi surface is closed, one should consider multiple patches which include the opposite side of the Fermi surface because fermions whose Fermi velocities are parallel or antiparallel with each other are all strongly coupled with the boson in the same momentum region. The theory which includes fermions with opposite Fermi velocities is given by

$$\mathcal{L} = \sum_j \sum_{s=\pm} \psi_{js}^*(\eta\partial_\tau - isv_{sx}\partial_x - v_{sy}\partial_y^2)\psi_{js} + \frac{e}{\sqrt{N}}\sum_{j,s} sa\psi_{js}^*\psi_{js} + a(-\partial_y^2)a, \tag{34}$$

where $\psi_{j-}(\psi_{j+})$ is the fermion whose velocity is parallel (antiparallel) to the x direction. It turns out that this theory is more complicated. For example, vacuum diagrams which include both ψ_+ and ψ_- also contribute to planar diagrams. An example is shown in Fig. 20. Those diagrams have the same enhancement factor as those which involve fermionic loops only on one side of the Fermi surface, if the curvatures of the Fermi surfaces are the same, that is, $v_{+x}/v_{+y}=v_{-x}/v_{-y}$. A complication arises because there is no constraint on internal frequencies such as Eq. (30) in the presence of fermions with opposite velocities. As a result, planar boson self-energy diagrams do not vanish in general and there exist UV divergences which are absent in the one patch theory at least in the large N limit. One possible scenario is that although there are UV divergences in individual diagrams, they cancel with each other and the coupling does not run. This scenario is consistent with the explicit two-loop calculation.[13] If this is the case, we will obtain a similar picture as the one patch theory. The question on how to sum all planar diagrams still remains.

If the curvatures on the opposite sides of the Fermi surface do not match ($v_{+x}/v_{+y} \neq v_{-x}/v_{-y}$), diagrams which has mixed fermion loops like the one in Fig. 20 has smaller

enhancement factor because all fermions cannot stay on the Fermi surface because of the curvature mismatch. In this case one side of the Fermi surface which has a smaller curvature will be dominant and one can focus on one patch as we did in this paper.

ACKNOWLEDGMENTS

The author thanks Andrey Chubukov, Piers Coleman, Matthew Fisher, Yong Baek Kim, Hong Liu, and Olexei Motrunich for useful discussions. This work has been supported by NSERC.

[1] H. v. Löhneysen, A. Rosch, M. Vojta, and P. Wolfle, Rev. Mod. Phys. **79**, 1015 (2007).
[2] P. Coleman, in *Handbook of Magnetism and Advanced Magnetic Materials*, edited by H. Kronmuller and S. Parkin (John Wiley & Sons, New York, 2007), Vol. 1, pp. 95–148.
[3] P. Gegenwart, Q. Si, and F. Steglich, Nat. Phys. **4**, 186 (2008).
[4] B. I. Halperin, P. A. Lee, and N. Read, Phys. Rev. B **47**, 7312 (1993).
[5] P. A. Lee, N. Nagaosa, and X.-G. Wen, Rev. Mod. Phys. **78**, 17 (2006), and references therein.
[6] Y. Shimizu, K. Miyagawa, K. Kanoda, M. Maesato, and G. Saito, Phys. Rev. Lett. **91**, 107001 (2003).
[7] T. Itou, A. Oyamada, S. Maegawa, M. Tamura, and R. Kato, Phys. Rev. B **77**, 104413 (2008).
[8] P. W. Anderson, Science **235**, 1196 (1987); P. Fazekas and P. W. Anderson, Philos. Mag. **30**, 423 (1974).
[9] O. I. Motrunich, Phys. Rev. B **72**, 045105 (2005).
[10] S.-S. Lee and P. A. Lee, Phys. Rev. Lett. **95**, 036403 (2005).
[11] P. A. Lee and N. Nagaosa, Phys. Rev. B **46**, 5621 (1992).
[12] J. Polchinski, Nucl. Phys. B **422**, 617 (1994).
[13] Y. B. Kim, A. Furusaki, X.-G. Wen, and P. A. Lee, Phys. Rev. B **50**, 17917 (1994).
[14] C. Nayak and F. Wilczek, Nucl. Phys. B **417**, 359 (1994); **430**, 534 (1994).
[15] B. L. Altshuler, L. B. Ioffe, and A. J. Millis, Phys. Rev. B **50**, 14048 (1994).
[16] O. I. Motrunich and M. P. A. Fisher, Phys. Rev. B **75**, 235116 (2007).
[17] R. K. Kaul, M. A. Metlitski, S. Sachdev, and C. Xu, Phys. Rev. B **78**, 045110 (2008); R. K. Kaul, Y. B. Kim, S. Sachdev, and T. Senthil, Nat. Phys. **4**, 28 (2008).
[18] S.-S. Lee, P. A. Lee, and T. Senthil, Phys. Rev. Lett. **98**, 067006 (2007).
[19] V. Galitski and Y. B. Kim, Phys. Rev. Lett. **99**, 266403 (2007).
[20] G. 't Hooft, Nucl. Phys. B **72**, 461 (1974).
[21] S.-S. Lee, Phys. Rev. B **78**, 085129 (2008).
[22] One can ignore four fermion interactions which induce "nonlocal" interactions in the momentum space because they are irrelevant in the large N limit.
[23] L. B. Ioffe and A. I. Larkin, Phys. Rev. B **39**, 8988 (1989).
[24] Here, the UV cutoff refers to a cutoff in the frequency.
[25] R. Shankar, Rev. Mod. Phys. **66**, 129 (1994).
[26] S.-W. Tsai, A. H. Castro Neto, R. Shankar, and D. K. Campbell, Phys. Rev. B **72**, 054531 (2005).
[27] T. A. Sedrakyan and A. V. Chubukov, Phys. Rev. B **79**, 115129 (2009).
[28] Nonperturbative effects can be ignored as is shown in Ref. 21.
[29] N. Seiberg, Nucl. Phys. B **435**, 129 (1995).
[30] A. M. Polyakov, Nucl. Phys. B, Proc. Suppl. **68**, 1 (1998).
[31] J. M. Maldacena, Adv. Theor. Math. Phys. **2**, 231 (1998).
[32] S. S. Gubser, I. R. Klebanov, and A. M. Polyakov, Phys. Lett. B **428**, 105 (1998).
[33] E. Witten, Adv. Theor. Math. Phys. **2**, 253 (1998).
[34] S.-S. Lee, Phys. Rev. D **79**, 086006 (2009).
[35] H. Liu, J. McGreevy, and D. Vegh, arXiv:0903.2477 (unpublished).
[36] M. Cubrovic, J. Zaanen, and K. Schalm, Science **325**, 439 (2009).